








Large Eruptive and Confined Flares in Relation to the Solar Active Region Evolution

Fuyu Li^{1,2,3} , Changhui Rao^{1,2,4} , Huaning Wang^{2,5}, Xinhua Zhao³ , Nanbin Xiang⁶ , Linhua Deng⁷, Haitang Li⁸, and Yu Liu⁸ 

¹ National Laboratory on Adaptive Optics, Chengdu 610209, People's Republic of China; chrao@ioe.ac.cn

² Institute of Optics and Electronics, Chinese Academy of Sciences, P.O. Box 350, Chengdu 610209, People's Republic of China

³ Key Laboratory of Solar Activity and Space Weather, National Space Science Center, Chinese Academy of Sciences, People's Republic of China

⁴ University of Chinese Academy of Science, Beijing, People's Republic of China

⁵ Faculty of Electrical Engineering and Computer Science, Ningbo University, Ningbo 315000, People's Republic of China

⁶ Yunnan Observatories, Chinese Academy of Sciences, Kunming 650011, People's Republic of China

⁷ School of Mathematics and Computer Science, Yunnan Minzu University, Kunming 650504, People's Republic of China

⁸ School of Physical Science and Technology, Southwest Jiaotong University, 999, Chengdu 611756, Sichuan, People's Republic of China

Received 2024 September 27; revised 2024 October 21; accepted 2024 October 29; published 2024 November 11

Abstract

Solar active regions (ARs) provide the required magnetic energy and the topology configuration for flares. Apart from conventional static magnetic parameters, the evolution of AR magnetic flux systems should have nonnegligible effects on magnetic energy store and the trigger mechanism of eruptions, which would promote the prediction for the flare using photospheric observations conveniently. Here we investigate 322 large (M- and X-class) flares from 2010 to 2019, almost the whole solar cycle 24. The flare occurrence rate is obviously higher in the developing phase, which should be due to the stronger shearing and complex configurations caused by affluent magnetic emergences. However, the probability of flare eruptions in decaying phases of ARs is obviously higher than that in the developing phase. The confined flares were in nearly equal counts to eruptive flares in developing phases, whereas the eruptive flares were half over confined flares in decaying phases. Yearly looking at flare eruption rates demonstrates the same conclusion. The relationship between sunspot group areas and confined/erupted flares also suggested that the strong field make constraints on the mass ejection, though it can contribute to flare productions. The flare indexes also show a similar trend. It is worth mentioning that all the X-class flares in the decaying phase were erupted, without the strong field constraint. The decaying of magnetic flux systems had facilitation effects on flare eruptions, which may be consequent on the splitting of magnetic flux systems.

Unified Astronomy Thesaurus concepts: [Solar active regions \(1974\)](#); [Solar flares \(1496\)](#); [Solar coronal mass ejections \(310\)](#)

1. Introduction

Flare incidences vary with magnetic environments of active regions (ARs), powered by the free magnetic energy (H. Zirin & M. A. Liggett 1987; V. I. Abramenko 2005; D. P. Choudhary et al. 2013; H. Wang et al. 2017; A. S. Kutsenko et al. 2024; A. G. M. Pietrow et al. 2024). Magnetic classification and field configuration also significantly affect flare productions (E. B. Mayfield & J. K. Lawrence 1985; P.-X. Gao et al. 2014; M. Zhao et al. 2014; S. Yang et al. 2017; A. Singh et al. 2024). The complexity magnetic configuration, high flux, stronger shearing, and the long polarity reversal line make a positive contribution to flare productions (H. Zirin & M. A. Liggett 1987; K. D. Leka & G. Barnes 2007; S. Toriumi & S. Takasao 2017; S. Toriumi et al. 2017; X. L. Yan et al. 2018; Z. Huang et al. 2019; Y. Liu et al. 2023). Most of flares occur in ARs that exhibit a synchronous increase in both the magnetic helicity and the magnetic flux during their emergence (Z. Sun et al. 2024). The ARs with large changes in sunspot area are flare productive (D. P. Choudhary et al. 2013). Free magnetic energy in the corona alone may be insufficient to trigger the flare to occur; evolution of the magnetic field structure and energy in the low solar atmosphere is also crucial to the trigger mechanism of flares, which can be treated as the

precursor of eruptive events (X. Sun et al. 2012; D. P. Choudhary et al. 2013; J. T. Su et al. 2014; H. Wang et al. 2017). The complex photospheric network of the AR with δ -sunspots can give rise to the formation of a coronal sigmoid, where flux ropes erupt successively (T. Shimizu et al. 2014; P. Chatterjee et al. 2016; P. Gömöry et al. 2017; P. K. Mitra et al. 2018).

Flares and coronal mass ejections (CMEs), the most obvious solar activities, did not always happen simultaneously. So-called eruptive flares are those accompanied by CMEs, whereas confined flares are those not associated with CMEs (Y. J. Hou et al. 2018; E. Pariat et al. 2023; R. Zheng et al. 2023). Generally, we believed that flares only occur in ARs. CMEs can take place in ARs or quiet regions, since quiescent prominence eruptions, AR prominence eruptions, and solar flares all have the potential to cause CMEs (Y. Liu et al. 2009; P.-X. Gao et al. 2014; M. D. Kazachenko et al. 2017). ARs erupt or not are partially dependent on the relative value of magnetic nonpotentiality over the restriction of the background field (X. Sun et al. 2015). Stronger magnetic confinements were found in those ARs with a larger magnetic flux (J. K. Thalmann et al. 2012; T. Li et al. 2020). Confined flares tend to have larger values of the length of steep gradient polarity inversion line (T. Li et al. 2021). A new magnetic parameter of magnetic field proposed by T. Li et al. (2022) is also significant in distinguishing confined and eruptive flares. Flare occurrence rates are also relevant to the transformation of sunspot group types (K. Lee et al. 2012; K. Lee et al. 2016; A. E. McCloskey et al. 2016). Thus, apart from some static parameters of the



Original content from this work may be used under the terms of the [Creative Commons Attribution 4.0 licence](#). Any further distribution of this work must maintain attribution to the author(s) and the title of the work, journal citation and DOI.

Table 1
Flare Eruptive Conditions in the AR Developing and Decaying Phases

Class	Developing Phase			Decaying Phase			χ^2
	Confined	Eruptive	Rate	Confined	Eruptive	Rate	
M-class	110	102	48%	36	53	60%	3.283
X-class	6	11	65%	0	4	100%	1.976
Total Number	116	113	49%	36	57	61%	3.787
M-class FI	238.3	251.7	51%	71.9	156.7	69%	18.754
X-class FI	114.0	300.0	72%	0.0	50.0	100%	18.253
Total FI	352.3	551.7	61%	71.9	206.7	74%	16.042

Note. The chi-square test values are listed in the last column.

magnetic field, the evolution of the AR is also a more efficient characteristic for the flare production.

Following ever-growing space weather forecast requirements and development of artificial intelligence, it would be effective to explore the relationship between flare occurrences and photospheric magnetic field characteristics. The AR evolutions and flare eruptive/confined categories approach is explained in Section 2. Flare counts and flare indexes related with different phases of ARs evolutions are analyzed in Section 3.

2. AR Information and Flare Database

ARs are the complex and changing areas with strong magnetic fields in the solar disk, where eruptions take place frequently (X. Sun et al. 2015; R. Wang et al. 2023). Information of ARs, such as coordinate, area (associated sunspot group area), magnetic type, and so on, is provided by the website of the Space Weather Prediction Center, National Oceanic and Atmospheric Administration (SWPC/NOAA; <https://www.swpc.noaa.gov/products/solar-region-summary>). The area of the AR approximately quantizes the strength of the AR flux system. According to daily area record variation trends, we divided the AR evolution process into the developing phase and the decaying phase. The peak-value day was included in the developing phase. The majority of ARs are unimodal. For few double-peaked ARs, their peaked times are determined by smoothing with the areas in the day before and the day after. We employed 103 ARs, where big flares were located in solar cycle 24.

Flare is graded by the soft X-ray flux from the Geostationary Operational Environmental Satellite (GOES). Generally, flares and flare ribbons can be recognized easily in Solar Dynamics Observatory (SDO) observations. Combining the database RibbonDB presented by M. D. Kazachenko et al. (2017) with the GOES flare catalog, T. Li et al. (2020) demonstrated the big flare (larger than M1.0) catalog from 2010 to 2019, almost the whole round of solar cycle 24 (T. Li et al. 2022; A. Singh et al. 2024). Then, 322 big flare events (301 M- and 21 X-class) within 45° from the central meridian were recorded. To identify their CME association, T. Li et al. (2020) checked the CME catalog (N. Gopalswamy et al. 2009) of the Solar and Heliospheric Observatory (SOHO)/Large Angle and Spectrometric Coronagraph (https://cdaw.gsfc.nasa.gov/CME_list/; M. D. Kazachenko et al. 2017). If the CME onset time was within 90 minutes of the flare start time and the position angle of the CME in the same quadrant where the flare occurred, it was regarded as an eruptive flare. Moreover, the observations of the twin Solar Terrestrial Relations Observatory (R. A. Howard et al. 2008; M. L. Kaiser et al. 2008) also provide CME information

from a different viewing angle. If a global coronal EUV wave observed by the Atmospheric Imaging Assembly (J. R. Lemen et al. 2012) on board the SDO was associated with a flare, it was classified as an eruptive flare.

3. Results

3.1. Flare Erupting Situation along with AR Evolution

ARs, where flares occur, provide required magnetic energies. The amount of free magnetic energy and complexity configuration play a catalytic role in flare production (D. P. Choudhary et al. 2013; H. Wang et al. 2017). The more complicated ARs have a higher occurrence rate (P. L. Bornmann & D. Shaw 1994; J. Ireland et al. 2008). Since the evolution of magnetic field type had influence on flare rate (K. Lee et al. 2016; A. E. McCloskey et al. 2016), the flaring mechanism should be considered with AR evolutions but not only static magnetic parameters. Therefore, we carried out an investigation on the relationship between ARs' dynamic evolutions and flare occurrences.

The AR evolution process can be divided into the developing phase and the decaying phase, in which the magnetic flux system performs different characteristics in collision or splitting (H. N. Wang et al. 2022; F. Li et al. 2024). The flare accompanied with the CME is regarded as eruptive. Otherwise, it is a confined flare. In Table 1, 322 M- and X-class flares from 2010 to 2017 are counted separately in developing and decaying phases of ARs. More than 70% of flares happen in the developing phase (in Table 1). This could be consequent on the complex magnetic field caused by the emerging magnetic field in the developing phase (A. S. Kutsenko et al. 2024). The eruption rates of M- and X-class and total flares are approximately 48%, 65%, and 49% in developing phases, while they are 60%, 100%, and 61% in descending phases. Owing to the diversity of production mechanisms between the flare and the CME, the eruptive rate is not necessarily consistent with flare productions. As shown in Figure 1, the stored counts for eruptive and confined flares are 116 and 113 in the developing phase, approximately equal values. However, in the decaying phase, the eruptive flares are 57, obviously more than that 36 confined flares. The difference between eruption rates states that the magnetic flux diffuses of an AR and the overlying field weakening makes it more likely to erupt. What is interesting is that no X-class flare is confined in decaying phases. It means that the declined magnetic field has less constraint on the big flare eruption.

To describe flares accurately with their X-ray flux (V. I. Abramenko 2005; J. T. Su et al. 2014), here we define

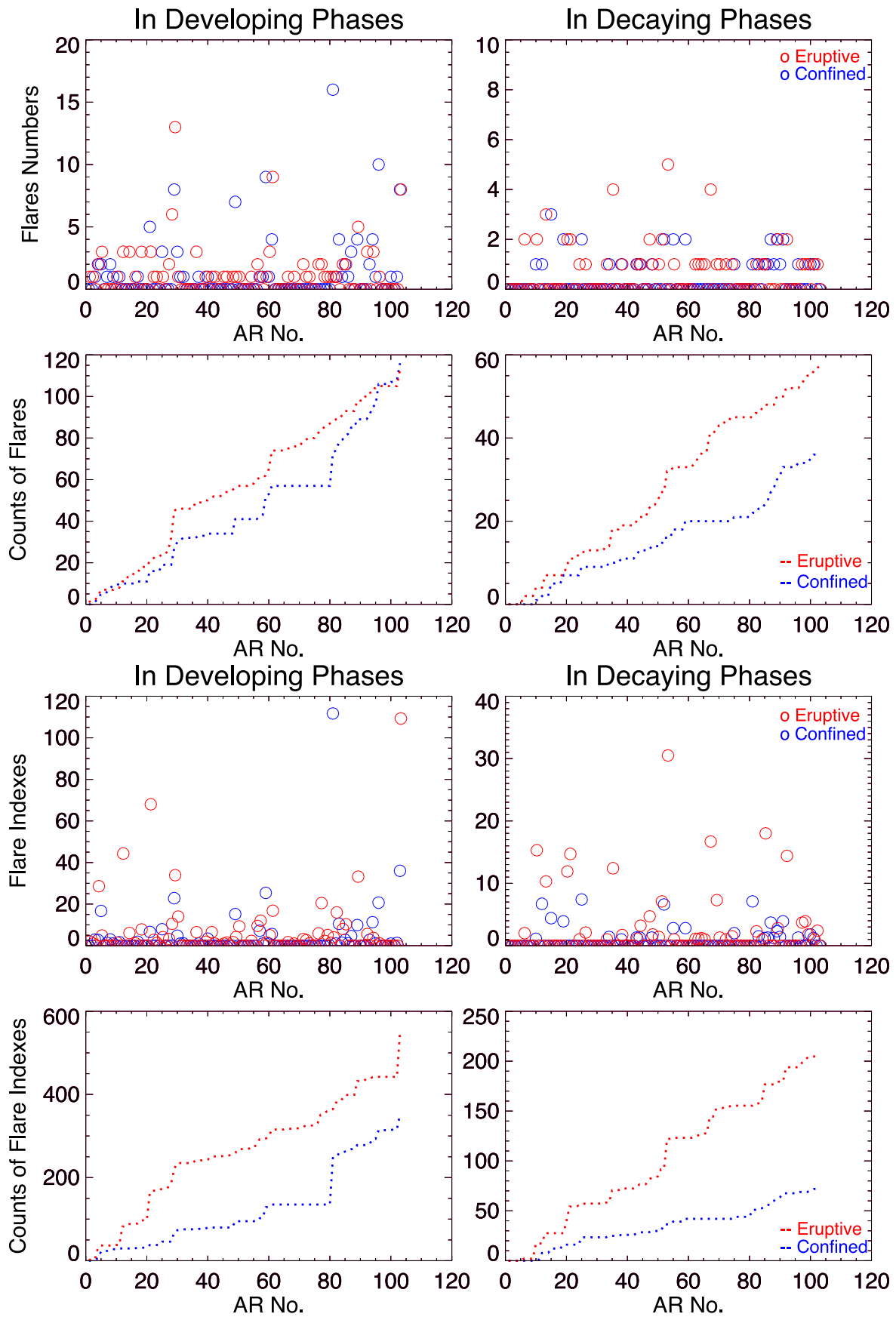


Figure 1. Flare outbreak situation in developing and decaying phases. The eruptive (red circles) and confined flare (blue circles) numbers for every ARs and the cumulative counts are exhibited in the four top panels. The conditions for flare indexes are shown in the four left panels. In decaying phases, the stored counts of eruptive flare quantities and indexes are significantly over those of confined flares.

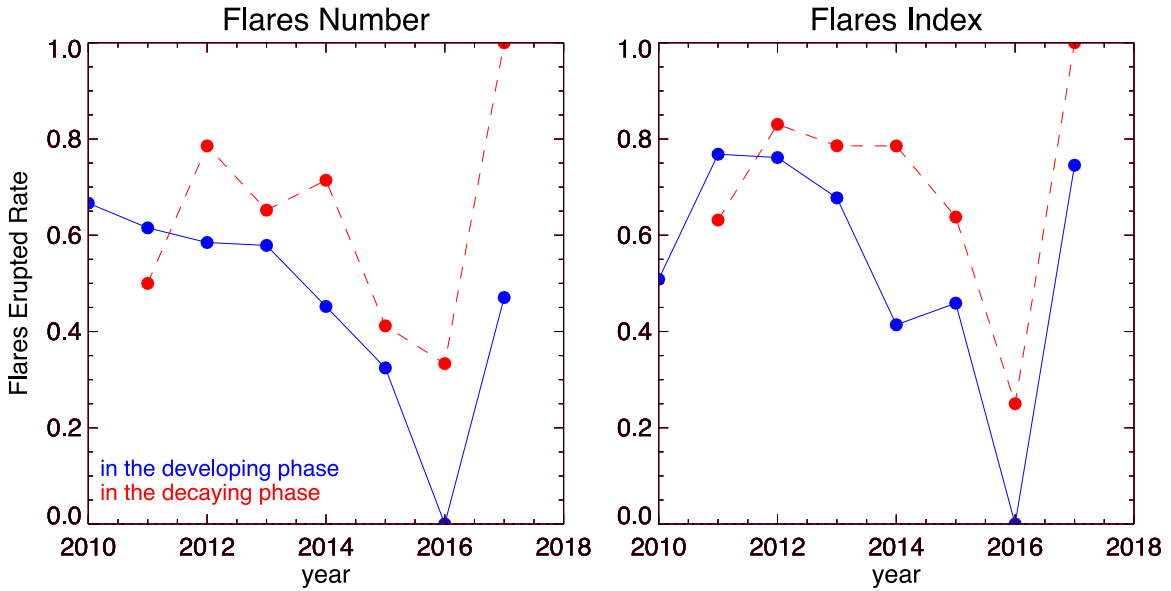


Figure 2. Yearly eruptive rate of flares in the AR developing phase and decaying phase computed from flare quantities (left panel) and flare indexes (right panel). The eruptive rate is obviously higher in decaying phase than in the developing phase.

Table 2
Yearly Counts of Eruptive and Confined Flare Quantities and Indexes in AR Developing and Decaying Phases

Year	Developing Phase				Decaying Phase			
	Confined Quantity	Eruptive Quantity	Confined Index	Eruptive Index	Confined Quantity	Eruptive Quantity	Confined Index	Eruptive Index
2010	1	2	2.9	3.0	0	0	0.0	0.0
2011	10	16	28.4	94.2	7	7	16.1	27.6
2012	22	31	45.2	144.3	3	11	8.8	43.1
2013	8	11	18.5	38.9	8	15	14.3	52.5
2014	40	33	167.6	118.4	6	15	14.6	53.5
2015	25	12	51.4	43.6	10	7	15.1	26.6
2016	1	0	1.0	0.0	2	1	3.0	1.0
2017	9	8	37.3	109.3	0	1	0.0	2.4
total	116	113	352.3	551.7	36	57	71.9	206.7

a simplified flare index for big flares:

$$FI = (10 \times \sum_n I_X + \sum_m I_M) / I_{M1.0}, \quad (1)$$

where n and m mean the sequence number of flares, and I_X and I_M are their peak soft X-ray flux of those X- and M-class flares, respectively. From the bottom panels in Figure 1, the cumulative counts of FI also exhibit a similar phenomenon that the eruptive rate appeared to be higher in decaying phases. As listed in Table 1, the eruption rates for M- and X-class and total flare indexes are approximately 51%, 72%, and 61% in developing phases, while they are clearly higher at 69%, 100%, and 74% in decaying phases. This result is consistent with that from flare counts.

To quantitatively assess the statistical significance level (P. R. Bevington & D. K. Robinson 2003), the chi-square test could be used:

$$\chi^2 = \sum_{i=1}^k \frac{(O_i - E_i)^2}{E_i}, \quad (2)$$

where O_i is the observed frequency and E_i is the expected frequency. The null hypothesis is that the confined/eruptive flare rate is the same in both the developing and decaying phases. As seen in Table 1, χ^2 , far greater than 1, denotes a significant difference between the developing and decaying phases. For M- and X-class and the total number of flares, their χ^2 is 3.283, 1.976, and 3.787, clearly over 1. For M- and X-class and total flare indexes, their χ^2 is 18.754, 18.253, and 16.042, much larger than 1. Thus, the advantage of eruptive rates in decaying phases compared to developing phases is statistically significant.

3.2. Yearly Confined/Eruptive Flares

Yearly sketches of 2010–2017 flares are listed in Table 2, including flare numbers and indexes. Figure 2 displays the yearly eruptive rates of flares in sequence, showing the disparity distinctly between the developing and decaying phases. It demonstrates that the flare eruption rates in the decaying phase are obviously higher than those in the developing phase. The sample quantity is infrequent in solar

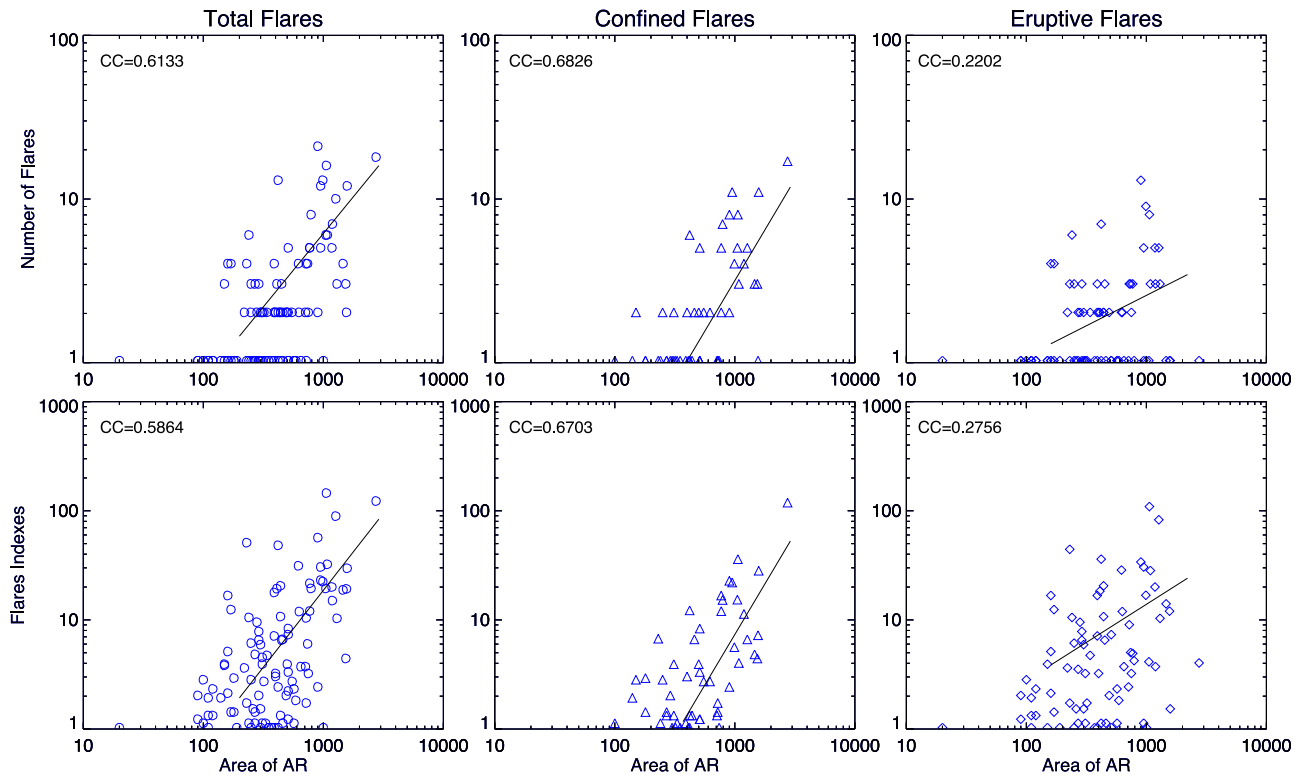


Figure 3. Relationship between flare eruption and sunspot group area in logarithmic coordinates. The three panels in the top row show the relation of the sunspot group area to the numbers of total flare, confined flares, and eruptive flares. Similar graphics for flare indexes are in the bottom line.

minimum. Nonetheless, it does not whittle the reliability of the whole conclusion about the eruptive rate being higher when ARs decline.

3.3. Flares and AR Areas

Larger ARs tends to cause stronger flares (I. Sammis et al. 2000; K. D. Leka & G. Barnes 2007; J. Muhamad et al. 2021). The sunspot group areas have positive correlation with the total unsigned magnetic fluxes (O. V. Chumak & H. Zhang 2003a, 2003b; A. Muñoz-Jaramillo et al. 2015; T. Sakurai & S. Toriumi 2023). However, a stronger magnetic environment does not certainly lead to more CME eruptions. For example, the great AR 12192 was flare productive but CME poor because of weaker nonpotentiality, a stronger overlying field, and smaller flare-related field changes (X. Sun et al. 2015; R. Zheng et al. 2023). In a strong magnetic field, separation velocity of flare ribbons is restrained, which is associated with a lower reconnection rate (M. D. Kazachenko et al. 2017; M. D. Kazachenko 2023). Figure 3 demonstrates the correlation between the AR areas and flares. The correlation coefficients of AR areas and the total flare numbers is 0.6133, at a 99.9% significance level. Moreover, the correlation coefficient for confined flares is 0.6826, suggesting a stronger correlation. Nevertheless, the correlation coefficient for erupted flares is 0.2202, which is statistically insignificant. The same information for flare indexes is plotted in the three bottom panels (Figure 3): the correlation coefficients are 0.5864, 0.6703, and 0.2756 for total flares, confined flares, and eruptive flares, respectively. Furthermore, flare indexes have similar linear correlations with AR areas as flare counts. Thus, the AR strength can facilitate the flares happening but confine CME eruption. This statistical result is consistent with the opinion

that the stronger overlying field could let the magnetic flux ropes be confined occasionally (Y. Wang & J. Zhang 2007; X. Sun et al. 2015; R. Zheng et al. 2023).

4. Conclusion and Discussion

To explore the influence of AR evolution on the flare eruption characteristic, we employed 322 M- and X-class flares from 103 associated ARs from 2010 to 2019. According to the common evolution of ARs, they are composed of the developing phase and the decaying phase. Original records for ARs, flares, and the CME were provided by the website of SWPC/NOAA, GOES, and SOHO (Section 2). As shown in Table 1, the majority of big flares happened in the growth phase of ARs. This is consequent on the complex magnetic field configuration caused by the emerging magnetic field in the developing phase (A. S. Kutsenko et al. 2024). The more complicated ARs have higher flare production rates (P. L. Bornmann & D. Shaw 1994; J. Ireland et al. 2008). However, the eruption rate was obviously higher in the decaying phase (Figure 1). Combined with the CME list, flares were categorized into eruptive and confined flares. Presented in Figure 1, the stored count of eruptive flares is near to the confined in developing phases, whereas it is significantly more than confined flares in declining phases. This is also verified by the cumulative count of flare indexes. In Figure 2, the yearly sketch also demonstrates that the flare eruption rates in developing phases are distinctly higher. The distinction of eruption rates suggests that the splitting of magnetic flux systems when the AR diminished should be a vantage configuration for CME eruptions. What is interesting is that no X-class flare is confined in decaying phases. This means that

the declined magnetic fields have less constraint on the big flare eruptions.

The larger sizes of ARs are favorable for flare productions (S. Toriumi & H. Wang 2019). However, they have suppression effects on CME eruption, as shown in Figure 3. The relationship between AR area and the number of confined flares is more significantly correlative than the eruptive flares (Figure 3, with data listed in Table 2). In a strong magnetic field, the separation velocity of flare ribbons is suppressed, which makes the reconnection rate lower (M. D. Kazachenko et al. 2017). Thus, the magnetic emergence has contributions to flare occurrences, but the decaying of ARs increases the eruption rate. It gives an inspiration that the flare and the CME are two independent physical processes, even though sometimes they occur in steps. Flares happening means the active area energy releases, whereas CMEs are more about mass losses. The complexity and rapid evolution are also key to the generation of strong flares (S. Toriumi & H. Wang 2019), as well as CMEs. However, morphological and magnetic complexities may have different manifestations for flares and CMEs. Regarding the evolution, we concluded that the developing phases of ARs were conducive to flare production, whereas the decaying phases increased the occurrence of CMEs.

Acknowledgments

This work was supported by the National Natural Science Foundation of China (NSFC) grants 12203054 and 42474224, Project Supported by the Specialized Research Fund for State Key Laboratories (CAS), and Sichuan Science and Technology Program 2023NSFSC1349. SDO is a mission of NASA's Living With a Star Program.

Facilities: GOES, SDO.

ORCID iDs

Fuyu Li  <https://orcid.org/0000-0002-2569-1632>
 Changhui Rao  <https://orcid.org/0000-0001-8571-8502>
 Xinhua Zhao  <https://orcid.org/0000-0002-9977-2646>
 Nanbin Xiang  <https://orcid.org/0000-0001-9062-7453>
 Yu Liu  <https://orcid.org/0000-0002-7694-2454>

References

Abramenko, V. I. 2005, *ApJ*, **629**, 1141
 Bevington, P. R., & Robinson, D. K. 2003, *Data Reduction and Error Analysis for the Physical Sciences* (New York: McGrawHill)
 Bornmann, P. L., & Shaw, D. 1994, *SoPh*, **150**, 127
 Chatterjee, P., Hansteen, V., & Carlsson, M. 2016, *PhRvL*, **116**, 101101
 Choudhary, D. P., Gosain, S., Gopalswamy, N., et al. 2013, *AdSpR*, **52**, 1561

Chumak, O. V., & Zhang, H. 2003a, in *ESA Spec. Publ. 535, Solar Variability as an Input to the Earth's Environment*, ed. A. Wilson (Noordwijk: ESA), **79**
 Chumak, O. V., & Zhang, H.-Q. 2003b, *ChJAA*, **3**, 175
 Gao, P.-X., Li, T., & Zhang, J. 2014, *RAA*, **14**, 1289
 Gömöry, P., Balthasar, H., Kuckein, C., et al. 2017, *A&A*, **602**, A60
 Gopalswamy, N., Yashiro, S., Michalek, G., et al. 2009, *EM&P*, **104**, 295
 Hou, Y. J., Zhang, J., Li, T., Yang, S. H., & Li, X. H. 2018, *A&A*, **619**, A100
 Howard, R. A., Moses, J. D., Vourlidis, A., et al. 2008, *SSRv*, **136**, 67
 Huang, Z., Li, B., Xia, L., et al. 2019, *ApJ*, **887**, 221
 Ireland, J., Young, C. A., McAteer, R. T. J., et al. 2008, *SoPh*, **252**, 121
 Kaiser, M. L., Kucera, T. A., Davila, J. M., et al. 2008, *SSRv*, **136**, 5
 Kazachenko, M. D. 2023, *ApJ*, **958**, 104
 Kazachenko, M. D., Lynch, B. J., Welsch, B. T., & Sun, X. 2017, *ApJ*, **845**, 49
 Kutsenko, A. S., Abramenko, V. I., & Plotnikov, A. A. 2024, *RAA*, **24**, 045014
 Lee, K., Moon, Y. J., Lee, J.-Y., Lee, K.-S., & Na, H. 2012, *SoPh*, **281**, 639
 Lee, K., Moon, Y. J., & Nakariakov, V. M. 2016, *ApJ*, **831**, 131
 Leka, K. D., & Barnes, G. 2007, *ApJ*, **656**, 1173
 Lemen, J. R., Title, A. M., Akin, D. J., et al. 2012, *SoPh*, **275**, 17
 Li, F., Rao, C., Zhao, X., et al. 2024, *ApJS*, **271**, 34
 Li, T., Chen, A., Hou, Y., et al. 2021, *ApJL*, **917**, L29
 Li, T., Hou, Y., Yang, S., et al. 2020, *ApJ*, **900**, 128
 Li, T., Sun, X., Hou, Y., et al. 2022, *ApJL*, **926**, L14
 Liu, Y., Su, J., Xu, Z., et al. 2009, *ApJL*, **696**, L70
 Liu, Y., Welsch, B. T., Valori, G., et al. 2023, *ApJ*, **942**, 27
 Mayfield, E. B., & Lawrence, J. K. 1985, *SoPh*, **96**, 293
 McCloskey, A. E., Gallagher, P. T., & Bloomfield, D. S. 2016, *SoPh*, **291**, 1711
 Mitra, P. K., Joshi, B., Prasad, A., Veronig, A. M., & Bhattacharyya, R. 2018, *ApJ*, **869**, 69
 Muhamad, J., Nurzaman, M. Z., Dani, T., & Pamutri, A. R. 2021, *RAA*, **21**, 312
 Muñoz-Jaramillo, A., Senkpeil, R. R., Windmueller, J. C., et al. 2015, *ApJ*, **800**, 48
 Pariat, E., Wyper, P. F., & Linan, L. 2023, *A&A*, **669**, A33
 Pietrow, A. G. M., Cretignier, M., Druett, M. K., et al. 2024, *A&A*, **682**, A46
 Sakurai, T., & Toriumi, S. 2023, *ApJ*, **943**, 10
 Sammis, I., Tang, F., & Zirin, H. 2000, *ApJ*, **540**, 583
 Shimizu, T., Lites, B. W., & Bamba, Y. 2014, *PASJ*, **66**, S14
 Singh, A., Chaudhari, A., Sharma, G., & Singh, A. K. 2024, *RAA*, **24**, 025012
 Su, J. T., Jing, J., Wang, S., Wiegelmann, T., & Wang, H. M. 2014, *ApJ*, **788**, 150
 Sun, X., Bobra, M. G., Hoeksema, J. T., et al. 2015, *ApJL*, **804**, L28
 Sun, X., Hoeksema, J. T., Liu, Y., et al. 2012, *ApJ*, **748**, 77
 Sun, Z., Li, T., Wang, Q., et al. 2024, *A&A*, **686**, A148
 Thalmann, J. K., Pietarila, A., Sun, X., & Wiegelmann, T. 2012, *AJ*, **144**, 33
 Toriumi, S., Schrijver, C. J., Harra, L. K., Hudson, H., & Nagashima, K. 2017, *ApJ*, **834**, 56
 Toriumi, S., & Takasao, S. 2017, *ApJ*, **850**, 39
 Toriumi, S., & Wang, H. 2019, *LRSP*, **16**, 3
 Wang, H., Liu, C., Ahn, K., et al. 2017, *NatAs*, **1**, 0085
 Wang, H. N., Rao, C., Gu, N., Zhong, L., & Huang, X. 2022, *ApJ*, **939**, 49
 Wang, R., Jiang, J., & Luo, Y. 2023, *ApJS*, **268**, 55
 Wang, Y., & Zhang, J. 2007, *ApJ*, **665**, 1428
 Yan, X. L., Wang, J. C., Pan, G. M., et al. 2018, *ApJ*, **856**, 79
 Yang, S., Zhang, J., Zhu, X., & Song, Q. 2017, *ApJL*, **849**, L21
 Zhao, M., Chen, J., & Liu, Y. 2014, *SSPMA*, **44**, 109
 Zheng, R., Liu, Y., Zhang, L., et al. 2023, *ApJL*, **942**, L16
 Zirin, H., & Liggett, M. A. 1987, *SoPh*, **113**, 267